JOURNAL OF GEOPHYSICAL RESEARCH, VOL. 100, NO. C10, PAGES 20,565–20,577, OCTOBER 15, 1995

# Sea level variations induced by heating and cooling: An evaluation of the Boussinesq approximation in ocean models

George L. Mellor and Tal Ezer
Program in Atmospheric and Oceanic Sciences, Princeton University, Princeton, New Jersey

**Abstract.** In this paper a sigma coordinate ocean model is modified to remove the commonly used Boussinesq approximation so that the effect of thermal expansion is exactly included in the basic equations in order to cope with the seasonal heating cycle and the detection of climate change through variation in sea level height. Tests are performed to evaluate the differences between Boussinesq and non-Boussinesq calculations under different heating and cooling conditions and different model domains. For an idealized case of a flat bottom, shallow ocean basin without wind forcing, simulations of a warm eddy show that the non-Boussinesq dynamics have only a minor effect on the baroclinic current field. However, vertically averaged velocities, though small compared with the baroclinic velocities, are cyclonic for the Boussinesq calculation and anticyclonic for the non-Boussinesq calculation. The results indicate that global or closed basin Boussinesq models should be able to simulate most of the observed steric sea level changes on seasonal or climate timescales, when corrected by a spatially uniform, time-dependent factor calculated from the volume-averaged density change. The seasonal variation of the globally averaged sea level calculated from climatological data is small, about 1 cm. Variations in steric sea level in regional models, both Boussinesq and non-Boussinesq, may differ from those of global models owing to the unknown transport across their boundaries associated with the local heating and cooling. A spatially uniform, time-dependent correction, similar to that associated with thermal expansion, is proposed to account for transport across open boundaries of regional models. Variations of sea level obtained from a Boussinesq model of the Atlantic Ocean approximate the seasonal signal due to the heating/cooling cycle of each hemisphere as observed by satellite altimeter data.

## 1. Introduction

Variations of density $\rho$ in the world oceans are relatively small, usually less than $\pm$ 2.5% of the average density $\rho_o$. Therefore a common assumption in ocean dynamics, known as the Boussinesq approximation, is to ignore variations in density where $\rho$ appears as a coefficient but to take into account variations in $\rho$ in the gravitational buoyancy force. This approximation is valid when the vertical scale of motion is small compared with the vertical scales of variations in density (see, for example, *Veronis* [1973, chapter 4], *Gill* [1982, chapter 6], and *Greatbatch* [1994] for more discussion of this approximation). The Boussinesq approximation is therefore a common assumption in ocean models, e.g., the Bryan-Cox model [*Bryan*, 1969; *Cox*, 1984], the Semi-spectral Primitive Equation Model (SPEM) [*Haidvogel et al.*, 1991], and the Princeton Ocean Model (POM) [*Blumberg and Mellor*, 1987; *Mellor*, 1992]. This approximation, when applied to ocean models, implies that the seawater is incompressible so that volume rather than mass is conserved. Thus, for example, a motionless ocean which is uniformly heated at the surface will not experience sea level change. Recently, *Greatbatch* [1994] has raised concern that since variations in sea level associated with expansion or contraction of the water column due to density changes are missing from ocean models, they may not correctly simulate seasonal [*Pattullo et al.*, 1955] and climatic [*Church et al.*, 1991] changes in sea level. For example, seasonal variations in sea level are observed in the global ocean with tide gauges [e.g., *Tsimplis and Woodworth*, 1994] and satellite altimeters [*Stammer and Wunsch*, 1994] but may differ from ocean model simulations. Ocean models can simulate steric sea level changes associated with climatic changes in thermohaline structure as recently demonstrated by *Ezer et al.* [1995]. Coastal ocean models can also forecast variations in sea level; for example, an experimental, operational, coastal nowcast/forecast system for the U.S. east coast [*Aikman et al.*, 1995] shows considerable skill in the prediction of short-term, wind-driven, sea level variations. However, the processes associated with long-term, seasonal, and interannual variations due to heating and cooling need further understanding before they can be accurately predicted by ocean models.

Consider a closed basin. It is supposed that the non-Boussinesq sea level can be written as

$$\eta(x,y,t) = \eta_B(x,y,t) + \eta_E(t) + \eta_{GS}(x,y,t) \qquad (1)$$

where $\eta_B$ is the local sea level change due to the Boussinesq dynamics, $\eta_E(t)$ is due to expansion or compression of the water column and is equal to the area average of $-H\overline{\delta\rho}/\rho_0$, where $H(x, y)$ is the bottom topography and $\overline{\delta\rho}(x, y, t)$ is the vertical average of the density deviation from a reference density $\rho_0$. In an application of (1), $\eta_{GS}$ is unknown and neglected as a small error; it is, however, largely attributable to the so-called "Goldsbrough-Stommel gyres" [*Greatbatch*, 1994], a non-



Paper number 95JC02442.
0148-0227/95/95JC-02442$05.00

Boussinesq vortex stretching effect due to density change. The Goldsbrough-Stommel gyre, first introduced for the case of forcing by mass flux due to evaporation and precipitation, is discussed also by *Huang and Schmitt* [1993].

The hypothesis embodied in (1) is that $\eta_E$ is independent of the spatial variables, $x$ and $y$. For (1) to be useful, $\eta_{GS}$ should be small so that, for example, Boussinesq global models when compared with observations may be adjusted by a globally uniform, time-dependent $\eta_E(t)$. In other words, the local elevation change induced purely by density change in the continuity equation is rapidly distributed over the entire domain with a timescale $L/c$, where $L$ is the basin lateral scale and $c = (gH)^{1/2}$ is the barotropic wave speed. In the most simplified case of a motionless ocean with a uniform heating, $\eta = \eta_E$. The main objective of this paper is to test a non-Boussinesq model and to compare it with its Boussinesq counterpart.

It should be mentioned that here the term "non-Boussinesq" does not refer to the full non-Boussinesq dynamics, which might also include acoustic waves [*Veronis*, 1973]. In the equation of state used here [*Mellor*, 1991] the density is calculated from the salinity, potential temperature, and pressure, $\rho = \rho(S, T, \tilde{p})$, but the pressure is calculated from the hydrostatic relation using an approximate, temporally constant density. Therefore sound waves are filtered out in both the Boussinesq and the non-Boussinesq models.

In this paper, relatively idealistic, numerical model experiments are performed (i.e., a flat bottom ocean without wind forcing) in order to clearly understand the difference between Boussinesq and non-Boussinesq models. An additional objective is to study the application of the Boussinesq approximation to regional models and to evaluate means of correcting Boussinesq models for non-Boussinesq effects.

The paper is organized as follows: sections 2 and 3 describe the non-Boussinesq model equations and their numerical implementation into the Princeton model. In section 4 the model is tested for simple cases of heated or cooled pools of water, and in section 5 we discuss an Atlantic Ocean simulation. An estimate of the global averaged, seasonal sea level change is presented in section 6. Equation (1) is reexamined in section 7 and extended to include regional models with open boundaries. Section 8 provides a summary of the study.

Two appendices are included in this paper. The first derives the appropriate equations of motion for variable density models. The second appendix analyzes the Boussinesq and non-Boussinesq, linear responses to buoyancy forcing.

## 2. The Governing Equations

The turbulence Reynolds equations of motion for a compressible fluid are presented in appendix A; terms in the governing equations are subjected to scale analysis wherein turbulent fluctuations are assumed small relative to variations in (ensemble) mean properties. In addition, we invoke the boundary layer approximation which includes the hydrostatic approximation. The analysis justifies the fact that turbulent fluctuations in density may be ignored, leaving only the need to account for mean density variations. In appendix A, overbars are used to denote Reynolds averages (elsewhere in this paper, overbars will represent vertical averages); here we eliminate the overbars except on the vertical turbulence flux terms. Thus the approximate continuity, heat, momentum, and hydrostatic equations for density $\rho$; potential temperature $T$; velocities $u,v,w$; and pressure $p$ can be written,

$$\frac{\partial \rho}{\partial t^*} + \frac{\partial}{\partial x^*}(\rho u) + \frac{\partial}{\partial y^*}(\rho v) + \frac{\partial}{\partial z^*}(\rho w) = 0 \qquad (2)$$

$$\frac{\partial \rho T}{\partial t^*} + \frac{\partial}{\partial x^*}\left(\rho u\, T\right) + \frac{\partial}{\partial y^*}\left(\rho v\, T\right) + \frac{\partial}{\partial z^*}\left(\rho w\, T\right) = \frac{\partial}{\partial z^*}\left(-\rho\overline{w'T'} + \frac{R}{C_p}\right) + F_T \qquad (3)$$

$$\frac{\partial \rho(u,v)}{\partial t^*} + \frac{\partial}{\partial x^*}\left[\rho u(u,v)\right] + \frac{\partial}{\partial y^*}\left[\rho v(u,v)\right] + \frac{\partial}{\partial z^*}\left[\rho w(u,v)\right] + f\rho(-v,u) = -\left(\frac{\partial p}{\partial x^*}, \frac{\partial p}{\partial y^*}\right) + \frac{\partial}{\partial z^*}\left[-\rho\overline{w'(u',v')}\right] + F_{u,v} \qquad (4)$$

$$\rho g = -\frac{\partial p}{\partial z} \qquad (5)$$

$R$ is the penetrative radiation flux and $C_p$ is the specific heat. Treatment of the salinity equation is identical to (3); the radiation term is, however, absent and is therefore omitted. Lateral diffusion is represented by $F_T$ and $F_{u,v}$. An equation of state based on the UNESCO formula [*Mellor*, 1991] relating density to potential temperature, salinity, and pressure completes the equation set. To invoke the Boussinesq approximation set, $\rho$ = constant = $\rho_o$ everywhere in the above equations except in (5).

It should be noted at the outset that the more important consequence of density variability, aside from that in (5), resides in the first terms in (2) and (3). Density variations appearing in the coefficients of velocity are a lesser effect in the ocean; they would, of course, be more important if the model equations were applied to the atmosphere.

Anticipating a need in the next section, we now transform the equations to depth-scaled, sigma coordinates so that $t^* = t$, $x^* = x$, $y^* = y$,

$$z^* = \eta(x, y, t) + \sigma D(x, y, t) \qquad (6a)$$

$$D(x, y, t) \equiv H(x, y) + \eta(x, y, t) \qquad (6b)$$

where $H(x, y)$ is the bottom topography, and

$$\phi(x^*, y^*, z^*, t^*) = \phi(x, y, \sigma, t) \qquad (7)$$

where $\phi$ is any dependent variable. It therefore follows that

$$\frac{\partial \phi}{\partial \alpha^*} = \frac{\partial \phi}{\partial \alpha} - \frac{1}{D}\left(\frac{\partial \eta}{\partial \alpha} + \sigma\frac{\partial D}{\partial \alpha}\right)\frac{\partial \phi}{\partial \sigma}, \quad \alpha \equiv x, y, t \qquad (8)$$

$$\frac{\partial \phi}{\partial z^*} = \frac{1}{D}\frac{\partial \phi}{\partial \sigma} \qquad (9)$$

After insertion of (7), (8), and (9) into (2), (3), and (4) we obtain the transformed sigma coordinate version

$$\frac{\partial \rho D}{\partial t} + \frac{\partial}{\partial x}(\rho D u) + \frac{\partial}{\partial y}(\rho D v) + \frac{\partial}{\partial \sigma}(\rho \omega) = 0 \qquad (10)$$

$$\frac{\partial \rho DT}{\partial t}+\frac{\partial}{\partial x}(\rho DuT)+\frac{\partial}{\partial y}(\rho DvT)+\frac{\partial}{\partial \sigma}(\rho \omega T)$$

$$=\frac{\partial}{\partial \sigma}\left(-\rho\overline{w'T'}+\frac{R}{C_p}\right)+DF_T \qquad (11)$$

$$\frac{\partial}{\partial t}\left[\rho D(u,v)\right]+\frac{\partial}{\partial x}\left[\rho Du(u,v)\right]+\frac{\partial}{\partial y}\left[\rho Dv(u,v)\right]$$

$$+\frac{\partial}{\partial \sigma}\left[\rho\omega(u,v)\right]+f\rho D(-v,u)=-\rho Dg\left(\frac{\partial \eta}{\partial x},\frac{\partial \eta}{\partial y}\right)-D^2 g$$

$$\times\left[\int_\sigma^0\left(\frac{\partial \rho'}{\partial x}-\frac{\sigma'}{D}\frac{\partial D}{\partial x}\frac{\partial \rho'}{\partial \sigma}\right)d\sigma',\int_\sigma^0\left(\frac{\partial \rho'}{\partial y}-\frac{\sigma'}{D}\frac{\partial D}{\partial y}\frac{\partial \rho'}{\partial \sigma}\right)d\sigma'\right]$$

$$+\frac{\partial}{\partial \sigma}\left[-\rho\overline{w'(u',v')}\right]+DF_{u.v} \qquad (12)$$

and we define a new "vertical" velocity (actually, the volume flux normal to sigma surfaces) according to

$$\omega \equiv w-u\left(\sigma\frac{\partial D}{\partial x}+\frac{\partial \eta}{\partial x}\right)-\left(\sigma\frac{\partial D}{\partial t}+\frac{\partial \eta}{\partial t}\right) \qquad (13a)$$

$$\omega(x,y,0,t)=\omega(x,y,-H,t)=0 \qquad (13b)$$

More details about the formulation of sigma coordinate models and the numerical implementation are given by *Blumberg and Mellor* [1987] and *Mellor* [1992].

## 3. Model Implementation

The numerical model is the Princeton ocean model which is a sigma coordinate, free surface, primitive equation model with an imbedded turbulence closure scheme [*Blumberg and Mellor*, 1987; *Mellor*, 1992] and which heretofore used the Boussinesq approximation whereby density is held constant except in the hydrostatic equation (5).

It is fairly obvious from an examination of (10), (11) and (12) that the process of converting our Boussinesq model to a non-Boussinesq model is greatly simplified by defining new density-weighted velocities, $(\tilde{u},\tilde{v},\tilde{w})=(\rho u,\rho v,\rho w)$ a partial adoption of a suggestion by R. J. Greatbatch and Y. Lu (unpublished manuscript, 1994). Much of the coding is therefore unchanged. The principal problem is the need to cope with the tendency terms $\partial \rho D/\partial t$ and $\partial \rho DT/\partial t$ so that properties are conserved. We use a leapfrog time step, and so it is necessary to extrapolate $\rho$ for the forward time step, then determine $D$ from (10) and $T$ and $S$ from (11) at the forward time step. Finally, the density is corrected using the equation of state. The code has a switch so that it can execute either the Boussinesq algorithm, where $\rho=\rho_o$ in (10) to (12), or the non-Boussinesq algorithm.

## 4. Experiments With Idealized Heating and Cooling

### 4.1. A Heated Pool of Water

To gain experience with the new model, we compare Boussinesq and non-Boussinesq runs for the same problem. The model basin is a square of 1000 x 1000 km with grid sizes $\Delta x=\Delta y=50$ km and $\Delta\sigma=0.05$, for a total of 21 sigma layers. The bottom is flat and has a depth of 200 m (extrapolation of the results to a deeper basin will be discussed later). The sigma layers are therefore the same as $z$ levels. The Coriolis parameter $f$ = constant = $10^{-4}$ s$^{-1}$.

To damp out both internal and inertial waves, the horizontal viscosity and diffusivity is, for this horizontal resolution, at the fairly high value of 2000 m$^2$ s$^{-1}$. The model's turbulence closure scheme is turned off for this study and the vertical viscosity and diffusivity decrease linearly from the value $10^{-2}$ m$^2$ s$^{-1}$ at the surface to zero at the depth of 100 m.

In this application the density is a direct prognostic variable; that is, use (11) and set $\rho=\rho_o+\delta\rho\equiv 1000$ kg m$^{-3}$ + $T$. The initial condition is a homogeneous fluid with a density of $\rho_0$ and zero velocities. For the first 5 days of the run the density is de creased via the radiational sink term on the right side of (11) and is therefore equivalent to heating. Horizontally, the input of negative density has a Gaussian distribution, $\exp\{-[(x-x_0)^2+(y-y_0)^2]/(200\text{ km})^2\}$, about the center of the domain, $(x_o, y_o)$. Vertically, the input is uniform in the upper 100 m of water whereas the lower 100 m is not affected.

According to (10) and (13b), together with zero normal velocities on the lateral boundaries, the integrals, $\iiint D\,dA\,d\sigma$ and $\iiint \rho D\,dA\,d\sigma$ are conserved in the Boussinesq case and non-Boussinesq case, respectively. After the sink term has been removed at day 5, $\iiint D\,\delta\rho\,dA\,d\sigma$ and $\iiint \rho D\,\delta\rho\,dA\,d\sigma$ are conserved in the Boussinesq case and non-Boussinesq case, respectively, in accordance with (11) and (13b). These quantities are also conserved appropriately by the numerical models.

After the fifth day when the sink term is shut off, the volume or mass-averaged density has decreased by 0.074 kg m$^{-3}$ relative to the initial 1000 kg m$^{-3}$. For the Boussinesq case the area average of $D$ or $\eta$ is conserved so that the area average of $\eta$ is zero. For the non-Boussinesq case the area average of $\overline{\delta\rho D}$ is conserved; this means that

$$\eta_E=-H\left\langle\frac{\overline{\delta\rho}}{\rho_o}\right\rangle=200\text{ m}\frac{0.074}{1000}=0.0148\text{ m}$$

where the angle brackets denote an area average.

Figure 1 shows the surface elevation after 20 and 40 days for the Boussinesq and the non-Boussinesq cases. The decay of the warm eddy with time due to diffusion is evident in both cases. Note that in the Boussinesq case the increase in surface elevation at the center is balanced by the decrease in elevation elsewhere (elevation is negative outside the dashed contour in Figures 1a and 1c), so the area-averaged elevation is zero.

Figure 2 shows a cross section at the center of the domain for the Boussinesq (dashed line) and the non-Boussinesq (solid line) cases; also shown is the Boussinesq case (dotted line) where a uniform correction of $\eta_E$ = 1.48 cm has been added. This correction brings the sea level closer to the non-Boussinesq case (the maximum error is reduced from 1.8 to 0.3 cm) but differs from the non-Boussinesq case due to the missing Goldsbrough and Stommel gyre $\eta_{GS}$. (*Greatbatch* [1994] defines this as a solution where nonlinearity and friction are neglected, whereas here they are included). It should be mentioned that experiments (shown later) with upper ocean cooling instead of heating produced a very similar effect; one merely needs to turn Figure 2 upside down. Figure 3 shows midbasin transects of the density anomaly $\delta\rho(x,y,z)$ for the non-Boussinesq case for days 20 and 40.

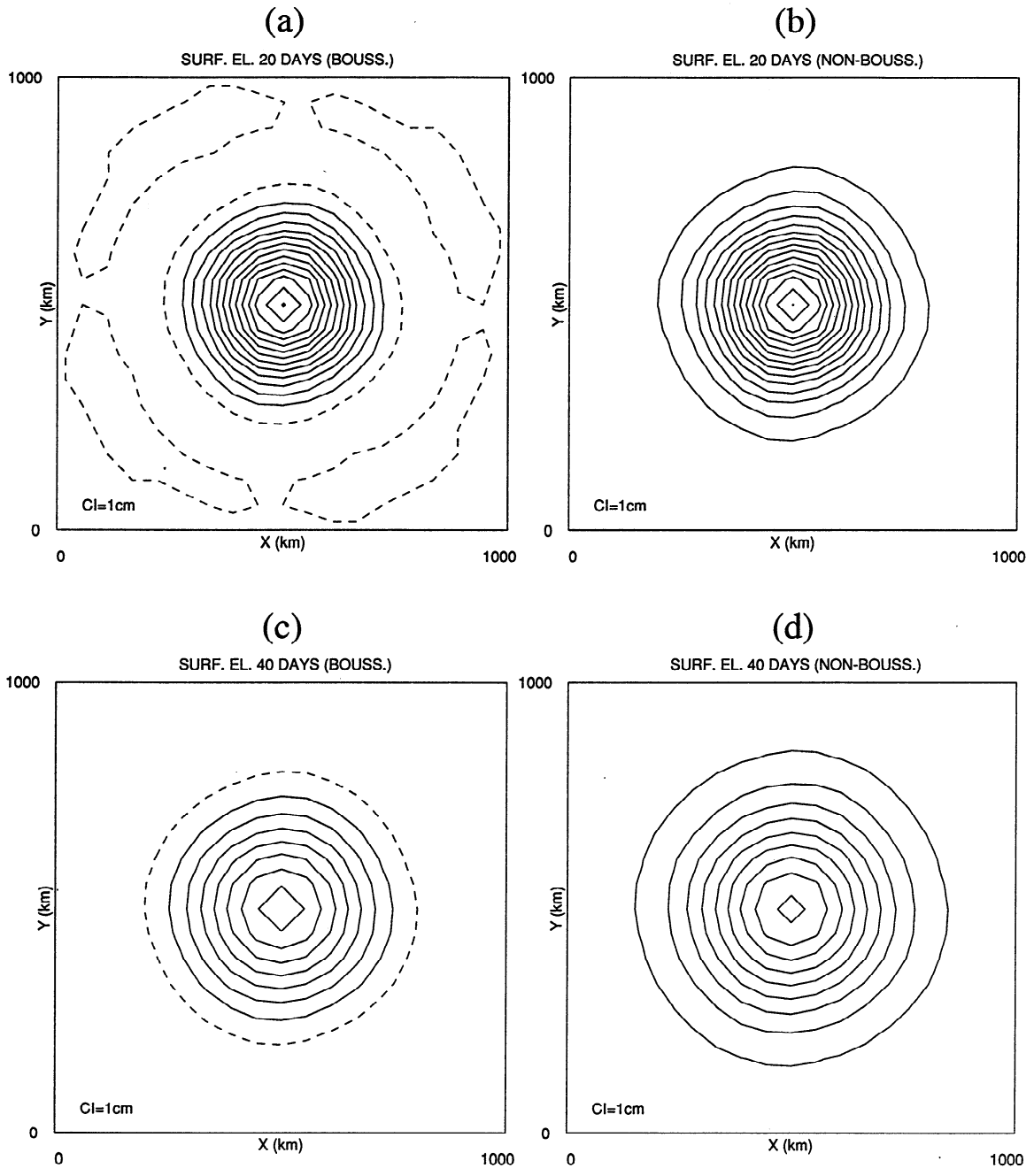


**Figure 1**. Surface elevation calculated by the (a) Boussinesq and by the (b) non-Boussinesq models after 20 days and the (c) Boussinesq and (d) non-Boussinesq models after 40 days, where the upper ocean warmed up during the first 5 days. The contour interval is 1 cm; dashed lines represent zero and negative contours, and the first contour in Figures 1b and 1d has a value of 1 cm.

Differences in the anomalies between the Boussinesq and non-Boussinesq models, associated with small changes in advection as shown later, are about 3 orders of magnitude smaller than the anomalies of either model. The decay of the eddy is again evident.

Cross sections of the transverse (swirl), $v$ component velocities for the Boussinesq and non-Boussinesq cases for day 20 are shown in Figure 4 (day 40 results are not shown; they are similar in structure to those of day 20 but with smaller amplitudes). The $v$ velocity component shows an anticyclonic circulation developed in the upper layers and a cyclonic circulation developed in the lower layers. Note that the non-Boussinesq effect is predominantly barotropic (Figure 4c). The difference between the two cases is quite small (the maximum Boussinesq error is about 0.3 cm $s^{-1}$ compared with the maximum flow of about 8 cm $s^{-1}$), and as indicated later, the error is much smaller in a deeper, more realistic basin.

We now look in more detail at the vertically averaged flow,

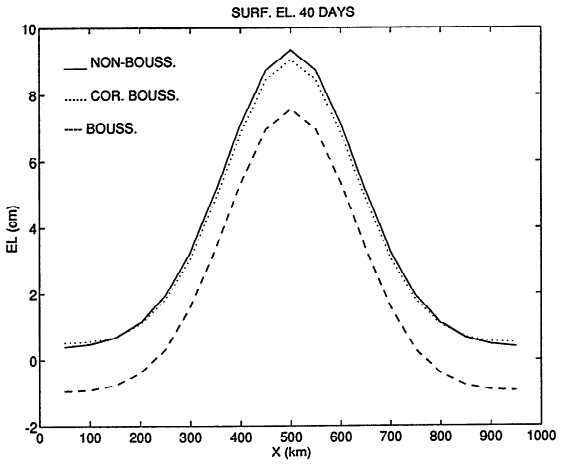


**Figure 2.** Surface elevation cross section at the center of the domain after 40 days. Solid, dashed, and dotted lines are for the Boussinesq, the non-Boussinesq, and the Boussinesq with uniform correction, respectively.

shown in the form of a stream function in Figure 5. While the Boussinesq case shows a (vertically averaged) weak, cyclonic circulation, the non-Boussinesq case shows a weak, anticyclonic circulation with additional, boundary-induced, subgyre structure. Note that the vertically averaged flow is smaller by about a factor of 20 than the maximum baroclinic flow; the maximum vertically averaged flows associated with Figures 5a and 5b are a cyclonic 0.34 cm $s^{-1}$ and a anticyclonic 0.21 cm $s^{-1}$, respectively. In this particular example the velocities in the upper and lower gyres (Figures 4a and 4b) almost balance each other, thus the remaining difference is of the same order as the non-Boussinesq, Goldsbrough-Stommel gyre (Figure 4c), about 0.2 cm $s^{-1}$. This error is much smaller than other errors in numerical models and is negligible compared with most wind-driven currents in the ocean.

To better understand this reversal in circulation, we examine the vertically integrated vorticity balance equation (see *Ezer and Mellor* [1994] for more detail on how the terms are calculated in the model). Figure 6 shows that the tendency and the Coriolis terms balance each other and both reduce in amplitude as the eddy decays. The signs of the two terms are, however, opposite in the non-Boussinesq case compared with the Boussinesq case. For this flat bottom case without surface and bottom friction, the leading terms in the vorticity equation are the relative vorticity tendency and Coriolis terms,

$$\frac{\partial}{\partial t}\left[\frac{\partial}{\partial x}\left(\overline{\rho v}\,D\right)-\frac{\partial}{\partial y}\left(\overline{\rho u}\,D\right)\right]-f\frac{\partial \bar{\rho} D}{\partial t},$$

plus the advection and diffusion terms. One can integrate the above equation, and since it is easy to justify the approximations, $D = H$ and $(\overline{\rho u}, \overline{\rho v}) = \rho_o(\overline{u}, \overline{v})$, on the left side one obtains the relative vorticity

$$\omega \equiv \frac{\partial \overline{v}}{\partial x}-\frac{\partial \overline{u}}{\partial y}=f\left(\frac{\delta\bar{\rho}}{\rho_o}+\frac{\eta}{H}\right)-\int(\text{adv.+diff.terms})dt$$

The Boussinesq relative vorticity is

$$\omega_B \equiv \frac{\partial \overline{v}_B}{\partial x}-\frac{\partial \overline{u}_B}{\partial y}=f\frac{\eta}{H}-\int(\text{adv.+diff.terms})dt$$

The difference in $\omega$ and $\omega_B$ and the reversal in the mean swirl is due to the term $\overline{\delta\rho}/\rho_o$, which subtracts from the vorticity stretching effect due to $\eta/H$.

A more extensive analysis of the Boussinesq and non-Boussinesq response to buoyancy forcing is included in appendix B. The appendix is, in fact, analytical justification for the decomposition of (1).

### 4.2. Adjacent Heated and Cooled Pools

In the previous experiment the most obvious correction needed in a Boussinesq model is the area-averaged, elevation adjustment

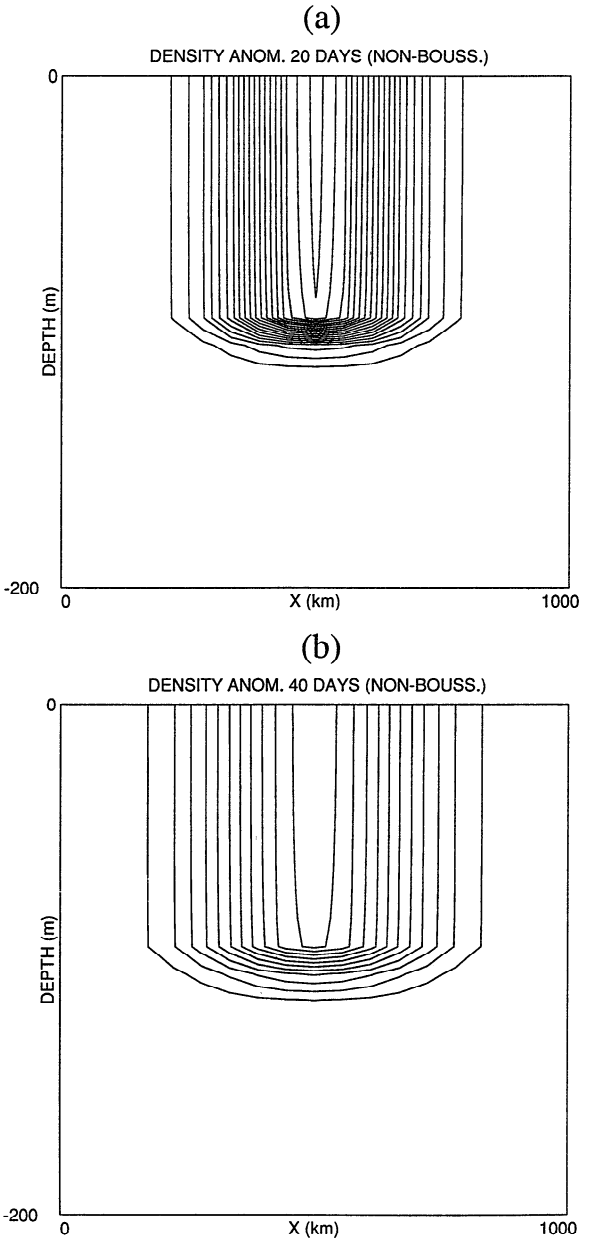


**Figure 3.** A cross section of $\delta\rho$ after (a) 20 days and (b) 40 days for the non-Boussinesq calculation. The contour interval is 1 kg $m^{-3}$; $\delta\rho = -2.0$ and $\delta\rho = -1.2$ kg $m^{-3}$ at the center of the eddy in Figures 3a and 3b, respectively, whereas $\delta\rho = 0$ in the outer and deeper regions.

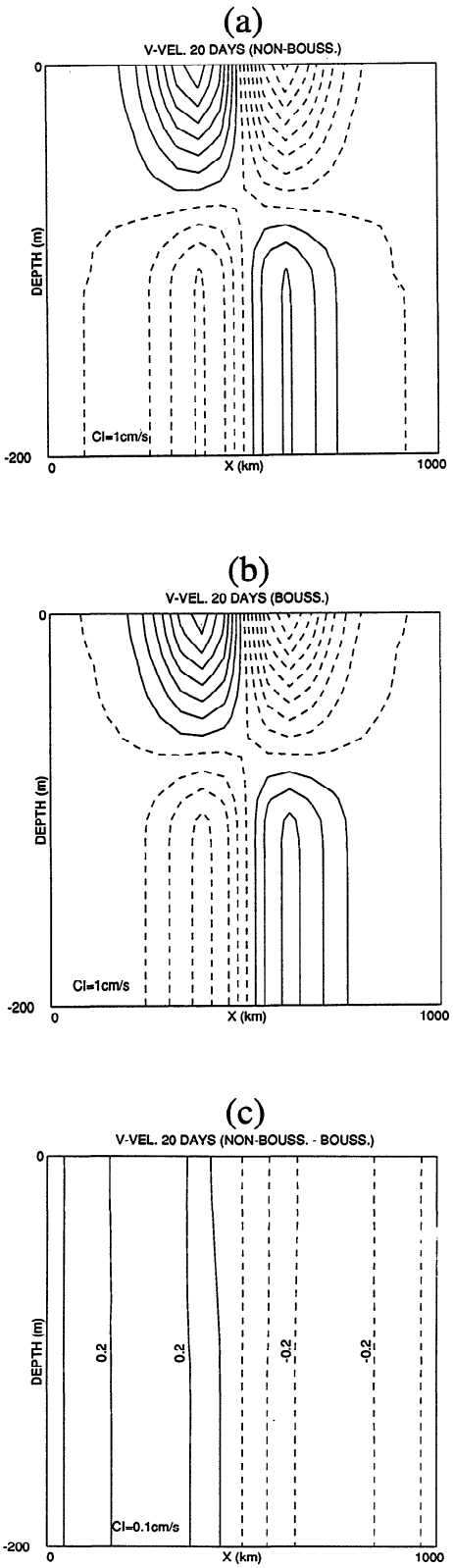


**Figure 4.** A cross section of the $v$ velocity component for (a) the non-Boussinesq calculation, (b) the Boussinesq calculation, and (c) the difference between the two cases after 20 days. Dashed lines represent negative contours; the first dashed line next to a solid line is the zero contour. The contour interval is 1 cm $s^{-1}$ in Figures 4a and 4b and 0.1 cm $s^{-1}$ in Figurte 4c.

$\eta_E$ (Figure 2) due to the change in volume-averaged density. However, in global (or closed basin) models, where one hemisphere is warmed while the other one is cooled, the average density change might be small. To test a case where $\eta_E = 0$, an experiment is performed as follows: a 1000 x 2000 km flat bottom ($H$ = 200 m), $f$-plane domain is used, where one half of the domain is cooled by the same amount as the other half is warmed (the heating/cooling are in a circular area as before), so the volume-averaged density does not change. In Figure 7 the surface elevation and the vertically averaged flow after 40 days is, in the northern half of the domain, similar to the previous experiments, but now there is a counterflow in the southern portion of the domain where density increases. The vertically averaged flow is again reversed between the Boussinesq and the non-Boussinesq cases as was the case with only one gyre. Note that the asymmetry between the heated and the cooled regions is due to the different dynamics of cold and warm eddies; for example, the cold eddy stretches farther downward while the warm eddy stretches farther outward with time. A comparison of surface elevation cross sections from south to north in Figure 8a reveals a spatially dependent, Boussinesq error $\eta_{GS}$ of about 1 cm or less. The results of this experiment differ from that of the single basin, single gyre by virtue of the flow exchange between the northern and southern portions of the basin.

In Figure 8b the non-Boussinesq, two-gyre experiment is also compared with non-Boussinesq cases representing separate regional (subbasin) models of a warm eddy (section 4.1) and a cold eddy. Now, let us pretend that the regional model is meant to simulate the flow and elevation of either subbasin which is a part of the whole basin. Since all models are non-Boussinesq, (1) offers no corrections for the regional models, so the difference in elevation between the regional subbasin models and the whole basin model in Figure 8b is due to the cross-basin transport which is missing from the regional models. An extension of (1) to account for cross-basin transport is obtained in section 7.

The experiments described here use a relatively shallow basin (simulating a shallow lake or continental shelf) where the Boussinesq effect is more pronounced. In experiments (not shown) with the same heating/cooling structure but with a 2000-m instead of 200-m bottom depth, the maximum Boussinesq error in surface elevation $\eta_{GS}$ after 40 days decreases from 0.3 to 0.03 cm. The latter is consistent with the fact that for a given heating or cooling the Goldsbrough-Stommel elevation is proportional to $H^{-1}$ as shown in appendix B.

## 5. The Atlantic Ocean

An example from a realistic Boussinesq model (with bottom topography and surface wind and heat fluxes) of the Atlantic Ocean is used to test if the seasonal cycle of sea level can be simulated. The Princeton ocean model in the Atlantic configuration has a horizontal resolution of about 20 to 100 km (with higher resolution in the Gulf Stream and the Antarctic circumpolar regions) and 16 sigma levels. The seasonal surface forcing is derived from the monthly climatologies based on the Comprehensive Ocean-Atmosphere Data Set (COADS) (see *Ezer and Mellor* [1994] for more detail); the inflow/outflow of the Antarctic Circumpolar Current (ACC) is prescribed and equal to a temporally invariant, total transport of 135 Sv (1 Sv = $10^6 m^3$ $s^{-1}$). The *Levitus* [1982] climatology has been used as an initial

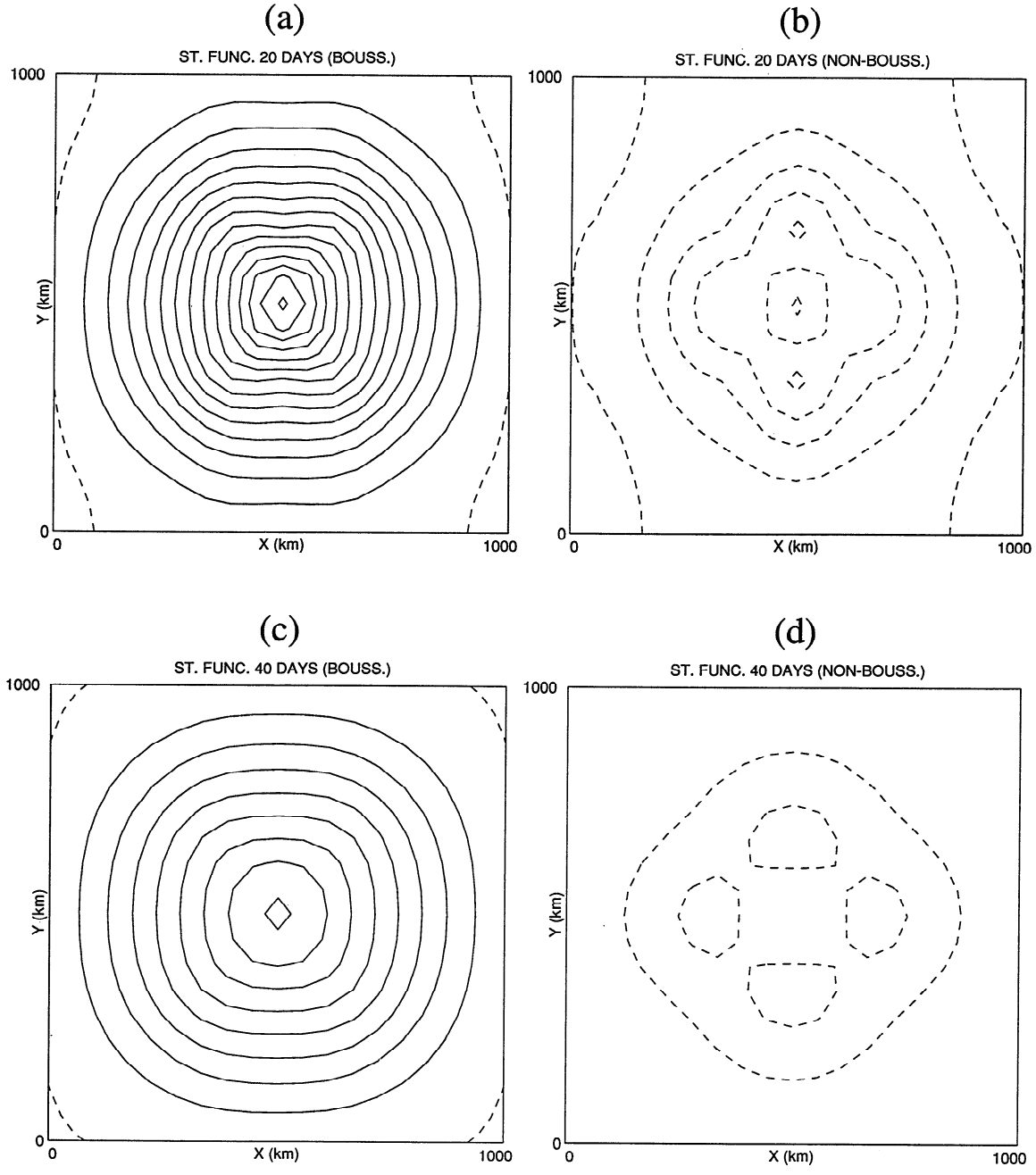


**Figure 5.** Vertically averaged stream function for the (a) Boussinesq and the (b) non-Boussinesq models after 20 days and the (c) Boussinesq and (d) non-Boussinesq models after 40 days. The contour interval of the stream function is $10^4 m^3 s^{-1}$. Solid and dashed contours represent cyclonic and anticyclonic circulation, respectively.

condition. The mean surface elevation obtained from the last 5 years of a 10-year run is shown in Figure 9. About a 1-m drop of sea level across the Gulf Stream and about a 1.6-m drop across the ACC are quite realistic features of the model. Further discussions and analyses of this model are left for other studies; here only the seasonal sea level signal (during one of the simulated years) is discussed.

The area-averaged elevation over each hemisphere (between 66°N and 66°S) is compared with observations from the TOPEX/POSEIDON altimeter in Figure 10a. The altimeter data are based on a 2° x 2° analysis of each repeat cycle (in 10-day intervals) calculated for 1993 (see *King et al.* [1994] and *Stammer and Wunsch* [1994] for more detail). The altimeter data are noisier than the model, which does not resolve eddies in most of the domain and is forced by smooth climatological surface data. However, one can see a clear seasonal signal in the Boussinesq model. The amplitude of this signal is comparable to that derived from the altimeter data for the South Atlantic but is underestimated for the North Atlantic region. The amplitude of the difference between the hemispheres is larger for the observa-

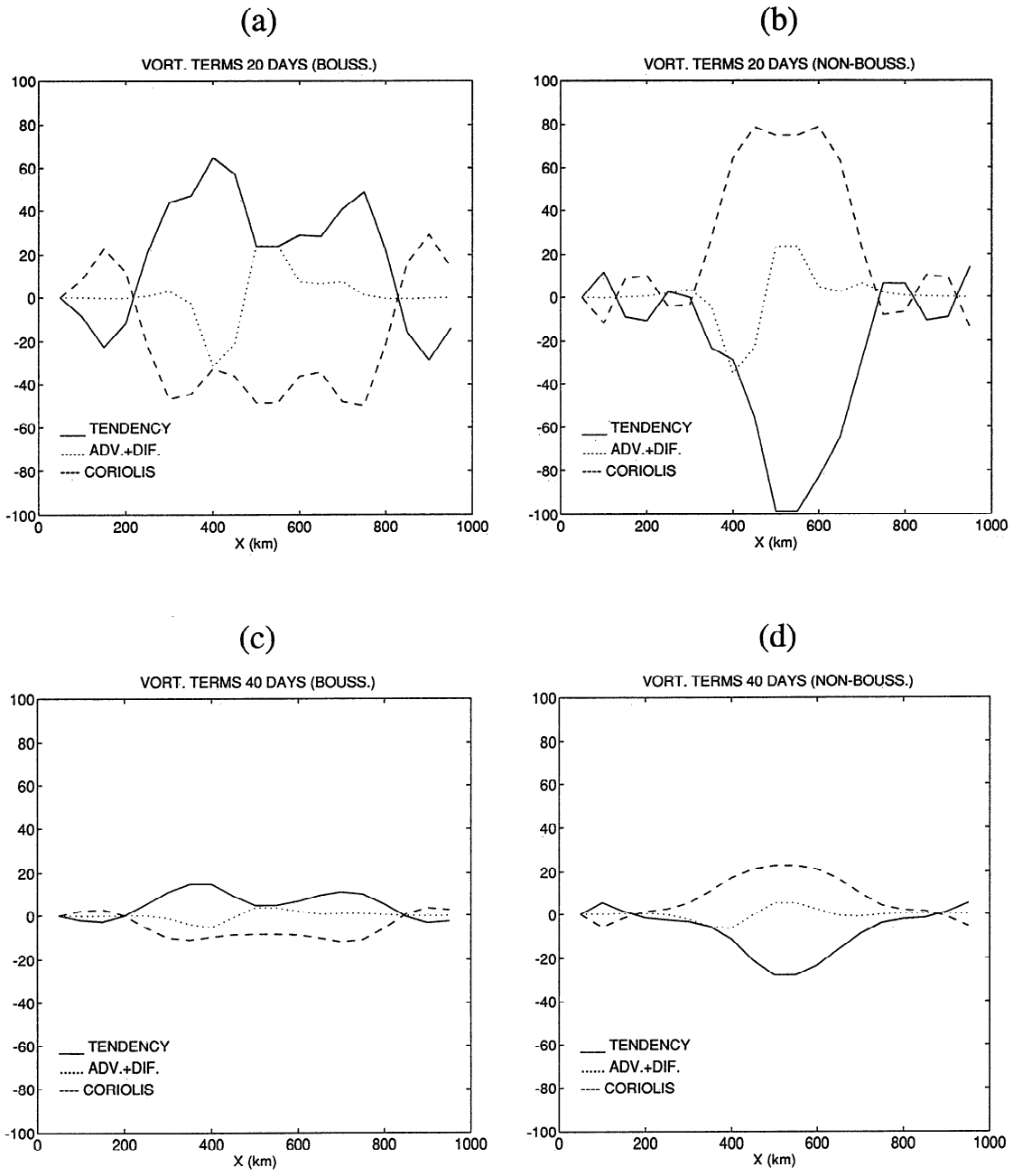


**Figure 6.** The leading terms in the vertically averaged vorticity balance equation (in units of $10^{-12}$ m s$^{-2}$) across the center of the domain for the (a) Boussinesq and the (b) non-Boussinesq models after 20 days and the (c) Boussinesq and (d) non-Boussinesq models after 40 days. The solid, dashed, and dotted lines represent the tendency, the Coriolis, and the advection and diffusion terms, respectively.

tions than for the model. In addition to model and observation error, this could be due to inadequacy in the climatological forcing or, less likely, interannual differences in surface heat flux. The expected thermal expansion elevation change calculated from the average density integrated over the North Atlantic (0 < latitude < 66°N), the South Atlantic (66°S < latitude < 0), and for the entire model domain is shown in Figure 10b. The model results in Figure 10a have been corrected for $\eta_E$ (Figure 10b, dotted line). However, this time-dependent uniform correction is small in this case, since the northern and the southern hemispheres are heated/cooled in opposite phases.

## 6. The Global Ocean

It is possible to evaluate the seasonal variations of $\eta_E$ from the *Levitus* [1982] analysis. Thus the result of calculating the global area average of $-H\,\overline{\delta\rho}/\rho_0$ is given in Figure 11. Also shown is an annual and semiannual Fourier fit to the data. The fact that $\eta_E \neq 0$ is, of course, due to the asymmetry between the northern and southern oceans; nevertheless, $\eta_E$ is small, about 1 cm. Therefore global Boussinesq models should require very little correction. The seasonal sea level variations for different oceanic basins have been estimated also by *Stammer and Wunsch* [1994] using the TOPEX/POSEIDON altimeter data.

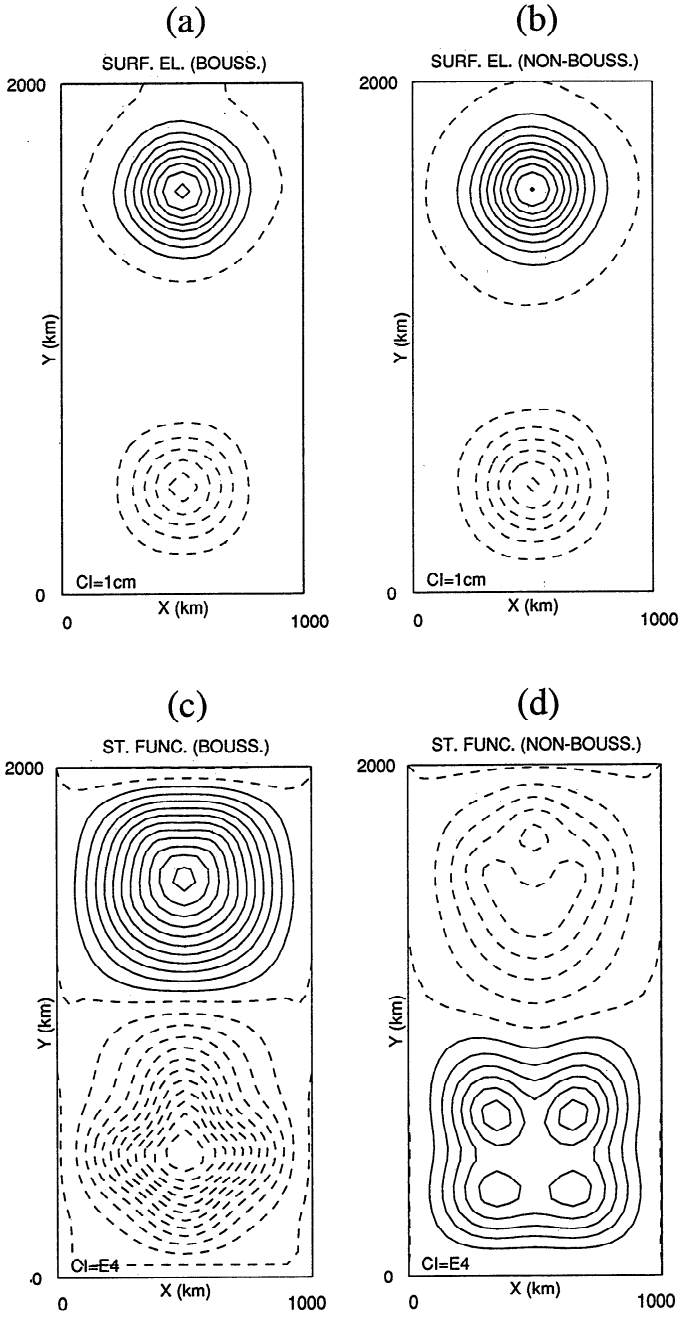


**Figure 7**. The surface elevation for the (a) Boussinesq and (b) non-Boussinesq models and the vertically averaged stream function for the (c) Boussinesq and the (d) non-Boussinesq models after 40 days, where the upper part of the domain is heated while the lower part is cooled. The contour interval is 1 cm for Figures 7a and 7b and $10^4$ m$^3$ s$^{-1}$ for Figures 7c and 7d.

## 7. Regional Models

In order to accommodate regional models, we review the basis for (1), now allowing for open boundaries. The vertically averaged continuity equation (2) may be written

$$\frac{\partial \overline{\rho} D}{\partial t} + \nabla \cdot \left( \overline{\rho \mathbf{V}} D \right) = 0$$

where $\nabla$ is a horizontal divergence operator and overbars denote vertical averages. Now $\overline{\rho} \equiv \rho_o + \overline{\delta\rho}$, to which we add $\overline{\mathbf{V}} = \overline{\mathbf{V}}_B + \overline{\delta \mathbf{V}}$. We consider $\eta$ and $\overline{\mathbf{V}}$ to be the "correct" elevation and vertically averaged velocity, whereas $\eta_B$ and $\overline{\mathbf{V}}_B$ are derived from Boussinesq physics but, in addition, may be a solution of a regional model which contains error due to the fact that velocities on the boundaries of the regional domain may be in error or, in fact, unknown. Here $\overline{\delta \mathbf{V}}$ is the difference between the vertically averaged, correct flow and the Boussinesq, regional flow. Thus

$$\frac{\partial}{\partial t}(\rho_o D) + \frac{\partial}{\partial t}\left(\overline{\delta\rho} D\right) + \nabla \cdot \left(\rho_o \overline{\mathbf{V}}_B D\right) + \nabla \cdot \left(\overline{\delta\rho}\, \overline{\mathbf{V}}_B D + \overline{\rho \delta \mathbf{V}} D\right) = 0$$

Now $\nabla \cdot \overline{\mathbf{V}}_B = \partial \eta_B / \partial t$ so that

$$\frac{\partial}{\partial t}\left( \eta - \eta_B + \frac{\overline{\delta\rho}}{\rho_o} D \right) + \nabla \cdot \left( \frac{\overline{\delta\rho}\, \overline{\mathbf{V}}_B}{\rho_o} D + \frac{\overline{\rho \delta \mathbf{V}}}{\rho_o} D \right) = 0 \qquad (14)$$

Finally, for the long timescale ( $<< L_x / \sqrt{gH}$ ) associated with heating and cooling cycles we make the jump from (14) to

$$\eta(x,y,t) = \eta_B(x,y,t) + \eta_E(t) + \eta_T(t) \qquad (15)$$

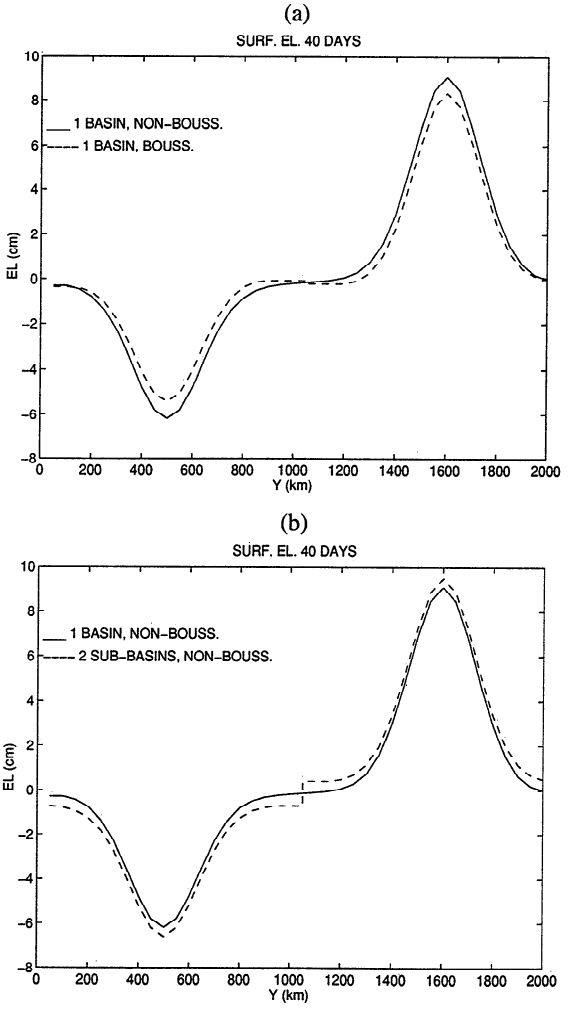


**Figure 8**. (a) Surface elevation in a cross section at the center of the $Y$ axis from south to north in Figures 7a and 7b. Solid and dashed lines represent the Boussinesq and the non-Boussinesq cases, respectively. (b) Non-Boussinesq cases. Solid lines represent calculations for the full basin model and dashed lines, where each gyre is separated from the other.

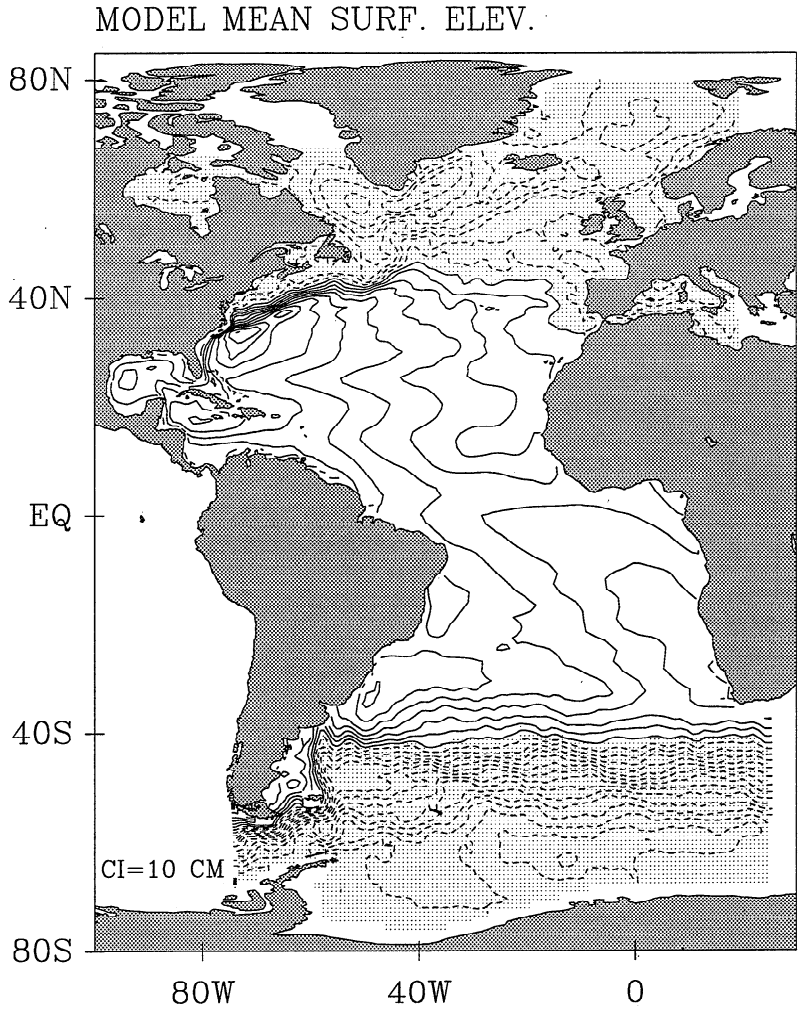


**Figure 9**. Five-year mean elevation obtained by the Boussinesq version of the Princeton ocean model driven by monthly climatological heat flux and wind stress. Contour interval is 10 cm; shaded areas and dashed contours represent negative values.

where we have neglected $\eta_{GS}(x,y,t)$ and

$$\eta_E \equiv -\left\langle \frac{\overline{\delta\rho}}{\rho_o} D \right\rangle \equiv -\frac{1}{A}\iint_A \frac{\overline{\delta\rho}}{\rho_o} D\,da \tag{16a}$$

$$\eta_T \equiv \int_0^t \frac{1}{A}\oint \frac{\overline{\delta\rho'\mathbf{V}'}_B + \overline{\rho'\delta\mathbf{V}'}}{\rho_o}\cdot\mathbf{n}\,Dds\,dt' \tag{16b}$$

so that both $\eta_E$ and $\eta_T$ are time dependent but are not dependent on $x$ and $y$. The divergence theorem is used to obtain (16b); the inner integrand is the flow through a lateral area element $Dds$; $\mathbf{n}$ is the unit vector normal to the area element. Generally, $\eta_T$ will be unknown and will have to be determined from empirical information external to the regional model.

Note that (15) can be extended to purely non-Boussinesq models, since $\eta = \eta_{NB} + \eta_T$. Therefore $\eta_T$ can provide a spatially independent, sea level correction to regional models as in Figure 8b.

## 8. Conclusions

The conventional governing equations of an ocean model have been modified to remove the Boussinesq approximation so that variations of steric sea level due to thermal expansion in processes such as the seasonal heating cycle [*Pattullo et al.*, 1955] and global climate change [*Church et al.*, 1991] are accurately included in the calculations. The numerical implementation partially conserves the basic structure of the ocean model by replacing the velocity component with velocity multiplied by density.

Experiments with different heating or cooling and different model domains have been performed to evaluate the Boussinesq approximation. The tests indicate that as suggested by *Greatbatch* [1994], a globally uniform, time-dependent correction of sea level can correct a Boussinesq solution so that it closely approximates the corresponding non-Boussinesq solution. This conclusion results from the fact that a non-Boussinesq model is able to dynamically adjust its surface elevation to spatially and temporally variable heating and cooling within a timescale shorter than seasonal or climatological timescales. The remaining error in the Boussinesq dynamics is associated with the so-called Goldsbrough-Stommel gyre due to vortex stretching effects associated with spatial heating patterns. An interesting result was that the vertically averaged flow was reversed by the non-Boussinesq dynamics in the idealized, flat bottom model and without wind forcing. However, the differences in sea level and

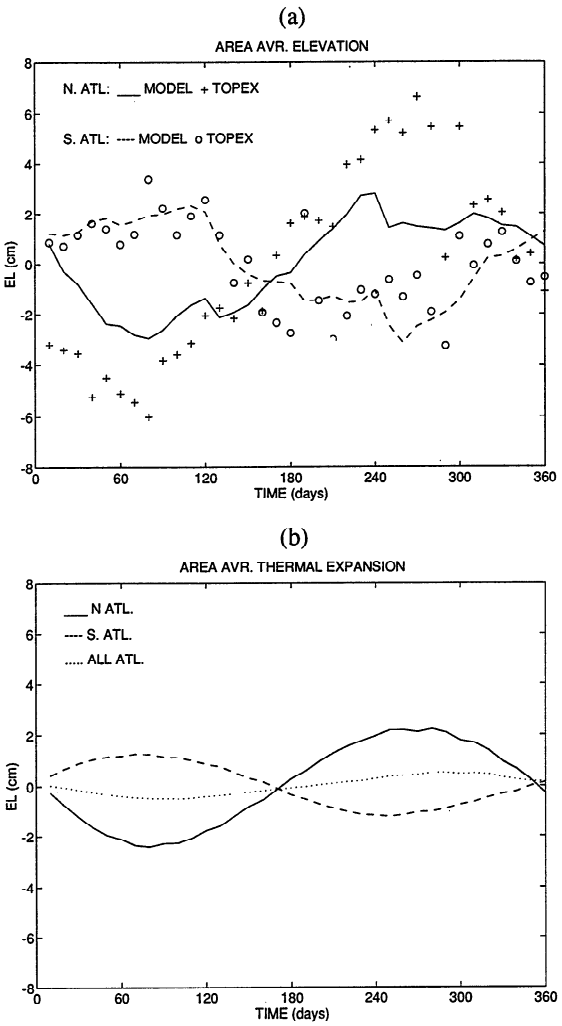


**Figure 10**. (a) The seasonal variations of the area-averaged surface elevation of each hemisphere (66°S to 66°N) from the Boussinesq model shown in Figure 9 (solid and dashed lines indicate averages over the North and the South Atlantic, respectively), and from the TOPEX/POSEIDON altimeter data (pluses and circles indicate averages over the North and the South Atlantic, respectively). (b) The area average of $-H\,\overline{\delta\rho}/\rho_0$ for the model North Atlantic (solid line) and South Atlantic (dashed line) and for the entire Atlantic Ocean (dotted line); the latter is $\eta_E$.

velocity compared with the Boussinesq result are usually negligibly small.

The net result for global models is that Boussinesq calculations can be corrected by a spatially independent, time-dependent function $\eta_E(t)$. The seasonal variation of this function is small, about 1 cm.

In the case of regional models an extension is needed, in the form of (15), to account for either Boussinesq or non-Boussinesq transport through open boundaries of ocean models. Once again, it is posited that Boussinesq calculations can be corrected by a spatially independent, time-dependent function. For example, it is clear that a spatially uniform $\eta_T$ could correct the subbasin response in Figure 8b. In the case of the Atlantic Ocean, Boussinesq simulation, the calculated $\eta_E$ (Figure 10b, dotted line) was small. We leave it to the reader to visualize a $\eta_T(t)$ correction which would improve agreement between model area-averaged sea level and the observations in Figure 10a.

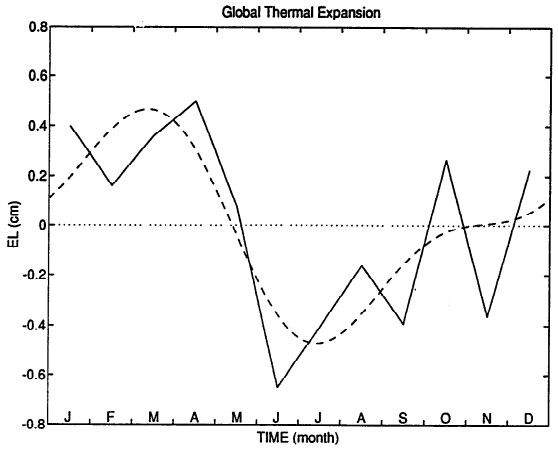


**Figure 11**. The globally averaged, seasonal variation of ocean elevation due to density changes, $\eta_E = -\langle H\overline{\delta\rho}/\rho_0\rangle$ calculated from the *Levitus* [1982] monthly climatology. The dashed curve is an annual and semiannual, Fourier fit to the data given by $\eta_E = 0.279\cos(\omega t) + 0.246\sin(\omega t) - 0.169\cos(2\omega t) + 0.017\sin(2\omega t)$, where $\omega = 2\pi$ / (12 months).

## Appendix A: The Reynolds Equations for a Compressible Fluid

The basic fluid dynamic equations for a low Mach number flow are

$$\frac{\partial \rho}{\partial t} + \frac{\partial}{\partial x_k}(\rho u_k) = 0 \tag{A1}$$

$$\frac{\partial \rho T}{\partial t} + \frac{\partial}{\partial x_k}(\rho u_k T) = -\frac{\partial q_k}{\partial x_k} \tag{A2a}$$

$$q_k = -\frac{k}{C_p}\frac{\partial T}{\partial x_k} \tag{A2b}$$

$$\frac{\partial \rho u_i}{\partial t} + \frac{\partial}{\partial x_k}(\rho u_k u_i) + \varepsilon_{ijk}\rho f_j u_k = -\frac{\partial p}{\partial x_k} + \frac{\partial \tau_{ki}}{\partial x_k} \tag{A3a}$$

$$\tau_{ki} = \mu\left(\frac{\partial u_i}{\partial x_k} + \frac{\partial u_k}{\partial x_i}\right) \tag{A3b}$$

We now decompose the independent variables into a mean (ensemble mean or time mean if the flow is stationary or spatial mean if the flow is homogeneous) variable plus a turbulence deviation so that

$$u = \overline{u} + u', \quad \rho = \overline{\rho} + \rho', \quad T = \overline{T} + T', \quad p = \overline{p} + p'$$

Then, the usual Reynolds' averaging yields

$$\frac{\partial \overline{\rho}}{\partial t} + \frac{\partial}{\partial x_k}\left(\overline{\rho}\,\overline{u}_k + \overline{\rho' u_k'}\right) = 0 \tag{A4}$$

$$\frac{\partial}{\partial t}\left(\overline{\rho}\,\overline{T} + \overline{\rho' T'}\right) + \frac{\partial}{\partial x_k}\left(\overline{\rho}\,\overline{u}_k\overline{T} + \overline{\rho' u_k' T'} + \overline{\rho}\,\overline{u_k' T'} + \overline{u}_k\overline{\rho' T'}\right) = 0 \tag{A5}$$

$$\frac{\partial}{\partial t}\left(\overline{\rho}\,\overline{u}_i + \overline{\rho' u_i'}\right) + \frac{\partial}{\partial x_k}\left(\overline{\rho}\,\overline{u}_k\overline{u}_i + \overline{\rho' u_k' u_i'} + \overline{\rho}\,\overline{u_k' u_i'} + \overline{u}_k\overline{\rho' u_i'}\right)$$

$$+ \varepsilon_{ijk} f_k\left(\overline{\rho}\,\overline{u}_k + \overline{\rho' u_k'}\right) = \overline{\rho} g_i - \frac{\partial \overline{p}}{\partial x_i} \tag{A6}$$

We neglect the molecular fluxes, $\tau_{ki}$ and $q_k$, although they are important in the very near vicinity of fluid boundaries and involve empirical, law-of-the-wall considerations which differ depending on whether the surface is smooth or rough. We have also neglected triple correlations in (A5) and (A6).

We now wish to evaluate the relative magnitude of the terms in the above equations through scale analysis. Therefore

$$\overline{\rho} \sim \rho_o + \delta\rho \tag{A7a}$$

$$(\overline{u},\overline{v},\overline{w}) \sim \delta u\ (1,1,\varepsilon_h) \tag{A7b}$$

$$\overline{T} \sim \delta T \tag{A7c}$$

$$\rho' \sim \delta\rho\ \varepsilon_t \tag{A7d}$$

$$(u',v',w') \sim \delta u\ \varepsilon_t \tag{A7e}$$

$$T' \sim \delta T\ \varepsilon_t \tag{A7f}$$

$$\partial/\partial t \sim 1/\delta t \tag{A7g}$$

$$\partial/\partial x, \partial/\partial y \sim 1/\delta x \tag{A7h}$$

$$\partial/\partial z \sim 1/(\varepsilon_h \delta x) \tag{A7i}$$

where the tilde symbol represents "order of". The $\delta$ represents expected variations in mean properties. Now interpret the left sides of (A7d-A7f) as rms values, and in the following discussion we will assume that correlation coefficients are of order 1. Thus $\overline{w'T'} = \delta u\,\delta T\,\varepsilon_t^2$, etc., where $\varepsilon_t$ will be assumed to be small. The parameter $\varepsilon_h$, defined in (A7b) and (A7i) and if assumed to be small, will invoke the boundary layer approximation and the hydrostatic approximation.

We focus on the continuity and temperature equation, since the former is critical to the purpose of this paper which would largely be defeated if the conservative nature of the latter were compromised. All of the terms in (A4) and (A5) are evaluated, and we eliminate those which are obviously small; the remainder are

$$\underbrace{\frac{\partial\overline{\rho}}{\partial t}}_{\frac{\delta\rho/\rho_o}{\delta t}} + \underbrace{\frac{\partial}{\partial x}(\overline{\rho}\,\overline{u}) + \frac{\partial}{\partial y}(\overline{\rho}\,\overline{v})}_{\frac{\delta u}{\delta x}\left(1+\delta\rho/\rho_o\right)} + \underbrace{\frac{\partial}{\partial z}\left[\left(\overline{\rho}\,\overline{w} + \overline{\rho' w'}\right)\right]}_{\frac{\delta u}{\delta x}\varepsilon_h\left(\left(1+\delta\rho/\rho_o\right)\varepsilon_h + \left(\delta\rho/\rho_o\right)\varepsilon_t^2\right)} = 0 \tag{A8}$$

$$\underbrace{\frac{\partial\overline{\rho}\,\overline{T}}{\partial t}}_{\frac{\delta T\left(1+\delta\rho/\rho_o\right)}{\delta t}} + \underbrace{\frac{\partial}{\partial x}\left(\overline{\rho}\,\overline{u}\,\overline{T}\right) + \frac{\partial}{\partial y}\left(\overline{\rho}\,\overline{v}\,\overline{T}\right)}_{\frac{\delta u\delta T}{\delta x}\left(1+\delta\rho/\rho_o\right)} + \underbrace{\frac{\partial}{\partial z}\left[\left(\overline{\rho}\,\overline{w} + \overline{\rho' w'}\right)\overline{T}\right]}_{\frac{\delta u\,\delta T}{\delta x\,\varepsilon_h}\left(\left(1+\delta\rho/\rho_o\right)\varepsilon_h + \left(\delta\rho/\rho_o\right)\varepsilon_t^2\right)} = \underbrace{\frac{\partial}{\partial z}\left(-\overline{\rho}\,\overline{w'T'}\right)}_{\frac{\delta u\,\delta T}{\delta x\,\varepsilon_h}\,\varepsilon_t^2} \tag{A9}$$

and where we include the scaling evaluation in the second line below each equation; all of these terms have been divided by $\rho_o$. For nonstationary flow one must have $\delta t \sim \delta x/\delta u$. The Boussinesq approximation is obtained if we let $\delta\rho/\rho_o \to 0$ so that $\overline{\rho} \to \rho_o$.

We next note that in order for the turbulent thermal flux term $\overline{w'T'}$ to be significant, then $\varepsilon_h = \varepsilon_t^2$. Therefore, if one wishes to retain terms of order $\delta\rho/\rho_o$ one should include the $\overline{\rho' w'}$ terms in the above two equations. However, the group, $\overline{\rho}\,\overline{w} + \overline{\rho' w'}$, appears in (A8) and (A9) in identical form so that it is simply possible to define a variable $\tilde{w}$, such that $\tilde{w} \equiv \overline{w} + \overline{\rho' w'}/\overline{\rho}$, and proceed with the simplified equations. These are cited in the main text as (2) and (3) without circumflexes or overbars. Equations (4) and (5) may be treated in similar fashion.

On the other hand, the same strategy could have been invoked at the level of (A4), (A5), and (A6). Thus one could define $\tilde{u}_k \equiv \overline{u}_k + \overline{\rho' u_k'}/\overline{\rho}$ and then proceed to eliminate small terms. However, (A8) and (A9) are still necessary to evaluate and identify the leading terms and to eliminate small terms which otherwise would increase the burden on the turbulence closure problem.

## Appendix B: Analysis of Boussinesq Versus Non-Boussinesq Flows

The principal dynamical consequences of non-Boussinesq density effects may, for easier comprehension, be represented by linear equations which for a flat bottom and after integrating with respect to $z$ become

$$\frac{\partial\overline{u}}{\partial t} - f\overline{v} = -g\frac{\partial\eta}{\partial x} - g\frac{\partial\phi}{\partial x} \tag{B1a}$$

$$\frac{\partial\overline{v}}{\partial t} + f\overline{u} = -g\frac{\partial\eta}{\partial y} - g\frac{\partial\phi}{\partial y} \tag{B1b}$$

where $\phi \equiv H^{-1}\int_{-H}^{0}\int_{z}^{0}\overline{\delta\rho'}/\rho_o\,dz'dz$ and

$$\frac{\partial\overline{u}}{\partial x} + \frac{\partial\overline{v}}{\partial y} + \frac{1}{H}\frac{\partial\eta}{\partial t} = -\frac{\partial}{\partial t}\left(\frac{\overline{\delta\rho}}{\rho_o}\right) \tag{B2}$$

The overbars denote vertical averages. If we integrate (B2) over an area bounded by a circuit on which the normal velocity component is zero and then integrate with respect to time, we obtain

$$\left\langle\frac{\eta}{H}\right\rangle = -\left\langle\frac{\overline{\delta\rho}}{\rho_o}\right\rangle \tag{B3}$$

where the brackets represent area averages. We have stipulated an initial rest state where $\eta = \overline{\delta\rho}/\rho_o = 0$.

Now differentiate (B1b) with respect to $x$, (B1a) with respect to $y$, subtract the two results, use (B2) and obtain potential vorticity conservation,

$$\frac{\partial\overline{\omega}}{\partial t} = f\frac{\partial}{\partial t}\left(\frac{\eta}{H} + \frac{\overline{\delta\rho}}{\rho}\right) - \beta\overline{v} \tag{B4a}$$

$$\overline{\omega} \equiv \frac{\partial\overline{v}}{\partial x} - \frac{\partial\overline{u}}{\partial y} \tag{B4b}$$

Next differentiate (B1a) with respect to $x$, (B1b) with respect to $y$, add the results, use (B2) again, and obtain

$$c^2\nabla^2\eta - \frac{\partial^2\eta}{\partial t^2} = H\frac{\partial^2}{\partial t^2}\left(\frac{\overline{\delta\rho}}{\rho_o}\right) + fH\overline{\omega} - \beta H\overline{u} - c^2\nabla^2\phi \tag{B5}$$

where $c \equiv \sqrt{gH}$. Next consider two regimes in parameter space where $\beta = 0$ and $\beta \neq 0$.

### B1. Steady Flow Cases Where $\beta = 0$

For $\beta = 0$, (B4a) can be integrated to give

$$\overline{\omega} = f\left(\frac{\eta}{H} + \frac{\overline{\delta\rho}}{\rho}\right) \tag{B6}$$

and (B5) reduces to

$$c^2\nabla^2\eta - \frac{\partial^2\eta}{\partial t^2} = H\frac{\partial^2}{\partial t^2}\left(\frac{\overline{\delta\rho}}{\rho_o}\right) + fH\overline{\omega} - c^2\nabla^2\phi \qquad \text{(B7)}$$

Consider a time when $\overline{\delta\rho}/\rho_o$ has departed from zero but thereafter is held constant, and transients have died out (the system needs some dissipation for this).The Boussinesq equations, emanating from (B2) for $\overline{\delta\rho}/\rho_o = 0$, are

$$\frac{\partial\overline{u}_B}{\partial x} + \frac{\partial\overline{v}_B}{\partial y} = 0 \qquad \text{(B8a)}$$

$$\overline{\omega}_B = f\frac{\eta_B}{H} \qquad \text{(B8b)}$$

$$c^2\nabla^2\eta_B - f^2\eta_B = -c^2\nabla^2\phi \qquad \text{(B8c)}$$

so that we can obtain nontrivial solutions, $\overline{u}_B, \overline{v}_B, \eta_B$, for this system forced by nontrivial $\phi(x, y)$. Note that $<\eta_B> = 0$.

Now set $\eta = \eta_B + \eta_r$ so that the remainder, non-Boussinesq solution is

$$\frac{\partial\overline{u}_r}{\partial x} + \frac{\partial\overline{v}_r}{\partial y} = 0 \qquad \text{(B9a)}$$

$$\overline{\omega}_r = f\left(\frac{\eta_r}{H} + \frac{\overline{\delta\rho}}{\rho}\right) \qquad \text{(B9b)}$$

$$c^2\nabla^2\eta_r - f^2\eta_r = f^2H\frac{\overline{\delta\rho}}{\rho_o} \qquad \text{(B9c)}$$

which is a system forced by $f^2\overline{\delta\rho}/\rho_o$. Note that $<\eta_r> = -H<\delta\rho/\rho_0> \equiv \eta_E$. The remainder, $\eta_{GS} \equiv \eta_r - <\eta_r>$, is attributable to the so-called Goldsbrough-Stommel gyre which from (B9c) is of the order of $L^2(f^2/c^2)H\overline{\delta\rho}/\rho_0$, where $L$ is the horizontal length scale of the variation in $\overline{\delta\rho}/\rho_0$. For the problem in Figures 1 to 4, $\eta_{GS}$ is smaller than $\eta_E$ by only a factor of 5 or so; however, for a given amount of buoyancy flux, $H\overline{\delta\rho}/\rho_0$ does not vary as $H$ is varied so that $\eta_{GS} \sim H^{-1}$. The result of the difference, $\overline{\omega} - \overline{\omega}_B = \overline{\omega}_r \cong f\overline{\delta\rho}/\rho_o$, is plotted in Figure 4c.

### B2. Steady Flow Cases Where $\beta \neq 0$

Consider steady state again. The only solution is $\overline{u} = \overline{v} = 0$ and $\eta = \phi - \langle\phi\rangle + \eta_E$.

Thus we obtain the well-known result that linearized, flat-bottomed ocean models yield zero vertically averaged velocities in the absence of wind stress curl.

### B3. Another Flow Case Where $\beta \neq 0$

*Greatbatch* [1994] considered the case, $\overline{\delta\rho}/\rho_o = Qt$, where $Q$ is independent of time. He assumes that $\phi = \partial\overline{u}/\partial t = \partial\overline{v}/\partial t = 0$ and $\partial\eta/\partial t = 0$, but in view of its definition, $\phi = HQt/2$, a steady state solution does not seem possible.

**Acknowledgments**. The research was supported by NOAA's Atlantic Climate Change Program, grant NA36GP0262; the Office for Naval Research (the Navy Ocean Modeling and Prediction Program), grant N00014-93-1-0037; by NOAA's Coastal Ocean Program; and by the computational support and facilities of NOAA's Geophysical Fluid Dynamics Laboratory.

## References

Aikman, F., G. L. Mellor, D. Rao, T. Ezer, D. Shenin, K. Bosley, and P. Chen, Toward an operational nowcast/forecast system for the U.S. east coast, in *Modern Approaches to Data Assimilation in Ocean Modeling*, edited by P. Malanotte-Rizzolli and D. Halpern, Elsevier, New York, in press, 1995.

Blumberg, A. F. and G. L. Mellor, A description of a three-dimensional coastal ocean circulation model, in *Three-Dimensional Coastal Ocean Models*, *Coastal Estuarine Sci.*, Vol. 4, edited by N. S. Heaps, 1-16, AGU, Washington, D.C., 1987.

Bryan, K., A numerical method for the study of the circulation of the world ocean, *J. Comput. Phys.*, *4*, 347-376, 1969.

Church, J. A., J. S. Godfrey, D. R. Jackett, and T. J. McDougall, A model of sea level rise caused by ocean thermal expansion, *J. Clim.*, *4*, 438-444, 1991.

Cox, M. D., A primitive equation, three-dimensional model of the ocean, *Tech. Rep. 1*, Ocean Group, Geophys. Fluid Dyn. Lab., NOAA, Princeton, N.J., 1984.

Ezer, T., and G. L. Mellor, Diagnostic and prognostic calculations of the North Atlantic circulation and sea level using a sigma coordinate ocean model, *J. Geophys. Res.*, *99*, 14,159-14,171, 1994.

Ezer, T., G. L. Mellor and R. J. Greatbatch, On the interpentadal variability of the North Atlantic Ocean: Model-simulated changes in transport, meridional heat flux, and coastal sea level between 1955-1959 and 1970-1974, *J. Geophys. Res.*, *100*, 10,559-10,566, 1995.

Gill, A. E., *Atmosphere-Ocean Dynamics*, 662 pp., Academic, San Diego, Calif., 1982.

Greatbatch, R. J., A note on the representation of steric sea level in models that conserve volume rather than mass, *J. Geophys. Res.*, *99*, 12,767-12,771, 1994.

Haidvogel, D. B., J. L. Wilkin, and R. Young, A semi-spectral primitive equation ocean circulation model using vertical sigma and orthogonal curvilinear horizontal coordinates, *J. Comput. Phys.*, *94*, 151-185, 1991.

Huang, R. X., and R. W. Schmitt, The Goldsbrough-Stommel circulation of the world oceans, *J. Phys. Oceanogr.*, *23*, 1277-1284, 1993.

King, C., D. Stammer, and C. Wunsch, The CMPO/MIT TOPEX/POSEIDON altimetric data set, *Rep. 30*, 42 pp., Dep. of Earth, Atmos. and Planet. Sci., Mass. Inst. of Technol., Cambridge, 1994.

Levitus, S., Climatological atlas of the world ocean, *NOAA Prof. Pap.*, *13*, 173 pp, U.S. Govt. Print. Off., Washington, D.C., 1982.

Mellor, G. L., An equation of state for numerical models of ocean and estuaries, *J. Atmos. Oceanic Technol.*, *8*, 609-611, 1991.

Mellor, G. L., User's guide for a three-dimensional, primitive equation, numerical ocean model, report, Program in Atmos. and Oceanic Sci., 35 pp., Princeton Univ., Princeton, N.J., 1992.

Pattullo, J., W. Munk, R. Revelle, and E. Strong, The seasonal oscillation in sea level, *J. Mar. Res.*, *14*(1), 88-156, 1955.

Stammer, D., and C. Wunsch, Preliminary assessment of the accuracy and precision of TOPEX/POSEIDON altimeter data with respect to the large-scale ocean circulation, *J. Geophys. Res.*, *99*, 24,584-24,604, 1994.

Tsimplis, M. N., and P. L. Woodworth, The global distribution of the seasonal sea level cycle calculated from coastal tide gauge data, *J. Geophys. Res.*, *99*, 16,031-16,039, 1994.

Veronis, G., Large scale ocean circulation, *Adv. Appl. Mech.*, *13*, 1-92, 1973.

G. L. Mellor and T. Ezer, Program in Atmospheric and Oceanic Sciences, P.O. Box CN710, Sayre Hall, Princeton University, Princeton, NJ 08544-0710. (e-mail: glm@splash.princeton.edu; ezer@splash.princeton.edu)

(Received November 15, 1994; revised April 11, 1995; accepted July 6, 1995.)